A Study of Twenty Years of Advanced Water Vapor Radiometer Data at Goldstone, California

David D. Morabito,* Daniel Kahan,* Meegyeong Paik,* Longtao Wu,† Elias Barbinis,* Dustin Buccino,* and Marzia Parisi*

ABSTRACT. — We examine ~20 years of brightness temperature measurements, including the meteorological data derived from these measurements, from the advanced water vapor radiometers (AWVRs) at the Deep Space Network (DSN) site of Goldstone, California in the Mojave Desert. This study reexamines 15 years of data from 2001 to 2015, reported in a previous article, and recent data from 2015 to 2021, which was used for training and testing as part of a machine learning (ML) weather forecasting study. This article describes the calibration and validation processes used to quantify the statistical behavior of the various data types over the ~20-year period. We also studied seasonal behavior by closely examining the statistics for a sample summer month and a sample winter month. We find that the data types show no significant trends during the ~20-year period, remaining within the ~1 K calibration uncertainty of the AWVR brightness temperatures. The 1.02 cm average of the annual integrated water vapor (IWV) extracted from the AWVR brightness temperatures is consistent with the 1.00 cm average from an earlier one-year study for Goldstone conducted in 1993–1994.

I. Introduction

Water vapor radiometers (WVRs) measure the sky brightness along a path through the atmosphere. This sky brightness includes contributions of atmospheric "noise" temperature and cosmic background. After removal of the cosmic background contribution, the remaining atmospheric noise temperature contribution is used to generate statistics of atmospheric attenuation and atmospheric noise temperature for telecommunications link budgets at frequency bands allocated for deep space communications such as Ka-band (32 GHz) [1]. We can also derive meteorological data types, such as integrated precipitable water vapor, liquid water content, and path delay, from the multi-frequency AWVR sky brightness temperature measurements.

The AWVR can track a spacecraft simultaneously with the 34 m ground antenna during a tracking pass to allow removal of water vapor contributions from the tracking Doppler

* Communications Architectures and Research Section.

† Instrument Software and Science Data Systems Section.

The research described in this publication was carried out by the Jet Propulsion Laboratory, California Institute of Technology, under a contract with the National Aeronautics and Space Administration.

data type. This process involves extracting the path delay from the multi-frequency AWVR brightness temperatures. The path delay has been used to calibrate or experimentally characterize atmospheric error sources in phase data gathered from radio science [2,3] and very long baseline interferometry (VLBI) experiments [4]. The TOPEX/Poseidon satellite, launched in 1992, carried a nadir-viewing radiometer at three similar frequencies (18, 21, and 37 GHz), providing range corrections due to water vapor with ~1 cm accuracy. For this instrument, Keihm, Janssen, and Ruf [1995] developed a statistical, two-step algorithm used for path delay retrieval [5].

By sampling multiple frequencies along or near the 22 GHz water vapor absorption line, additional data types can be extracted from the AWVR sky brightness measurements using retrieval coefficients derived from radiosonde data [6]. These data types include integrated precipitable water vapor, integrated liquid water content, and water vapor induced-path delay. Statistical inversion was employed to extract the water vapor products and liquid water content from the multifrequency brightness temperature measurements [7]. Such techniques include comparison of the radiometer estimates with measurements from radiosonde launches in the same locality or at least in a nearby proxy locality. Simultaneous VLBI and WVR experimental measurements on a 21 km baseline within the Deep Space Network (DSN) Goldstone, California tracking site demonstrated that WVRs removed a sizable contribution of tropospheric delay fluctuations from the VLBI data [4]. Review of the extraction of path delay from microwave radiometry can be found elsewhere in the literature [8].

The differenced path delay between the two spatially separated WVRs forms an additional data type that provides a measure of atmospheric decorrelation over the spatial distance, which can be used in arraying applications. Such statistics are routinely acquired by site test interferometers (STIs) at the DSN sites [9]. In August 2008, two AWVRs were deployed next to each antenna element of an STI in Goldstone, California, in order to validate the atmospheric nature of these measurements [10]. This study found that the spatial fluctuations measured by the WVR baseline were consistent with those measured by the STI, thus providing an added degree of validation.

A previous article [11] compares calculated atmospheric effects using different methods for the DSN and two Near Earth Network (NEN) sites that are commonly used in telecommunications links. Atmospheric attenuation estimated from International Telecommunication Union (ITU) models was compared with atmospheric attenuation derived from WVR measurements at the three DSN sites and found to be in reasonable agreement. A few discrepancies were believed to be consistent with higher uncertainties in the ITU models or their inputs, especially with the liquid content models (rain and clouds) at higher percentiles. The DSN attenuation statistics derived from WVRs [1] provided a good testbed in which to cross-compare against the statistics of atmospheric losses derived from ITU prediction methods.

A previous Goldstone AWVR study, covering 2001 to 2015, compared atmospheric data type statistics derived from AWVR data against ITU models [12]. A recent study motivated by exploring machine learning (ML) weather forecasting for flight operations [13] involved the addition of Goldstone AWVR data from 2016 to 2020. Another study

involved a comparison of atmospheric quantities derived from AWVRs and weather analysis data [14].

In this study, we examine and cross-compare the statistics and time-variability of the AWVR brightness temperature measurements, acquired between 2001 and 2021, and the meteorological data types derived from these measurements. The calibrated/validated AWVR data studied here are part of the training and testing data sets in a ML weather forecast system to predict atmospheric noise temperature (Tatm) at DSN tracking sites in support of deep-space missions [13]. The forecast model is trained with the National Centers for Environmental Prediction (NCEP) forecast and analysis data sets involving the Tatm derived from on-site AWVRs. Atmospheric noise temperature can be predicted up to 16 days ahead [13].

II. The AWVR Observations

In this section, we discuss the observations available from the AWVRs, as well as specific items relating to calibration, validation, and delivery of the data. The two AWVRs, designated AWVR-1 and AWVR-2, currently reside next to the 34 m diameter beam-waveguide (BWG) antenna Deep Space Station (DSS) 25 in Goldstone, California (Figure 1).

AWVR-2 has been located at Goldstone next to the 34 m diameter Ka-band capable antenna (designated DSS-25) since 2001 (except during repair/refurbishment periods). AWVR-1 was originally located in Goldstone along with AWVR-2 during 1999 to 2000, during which it was involved in a validation effort performing interferometry between DSS-13 and DSS-15 [15]. The AWVRs were moved alongside DSS-25 to support the Cassini gravitational wave experiments in the early 2000s. In June 2004, AWVR-1 was moved to

Figure 1. AWVR-2 (foreground) and AWVR-1 (background to the right) with 34 m DSS-25 BWG.

Madrid, Spain to support VLBI experiments between Goldstone and Madrid [16], and then moved back to Goldstone, alongside AWVR-2, in 2016 to provide redundancy and back-up for the Juno Ka-band mission [3,17]. Acquisition of Goldstone data from AWVR-1 resumed in September 2017.

For this study, we used data acquired near zenith at elevation angles > 80° to avoid the "Sun-in-beam" problem encountered at lower elevation angles during some spring and summer tipping curves. Here, sizeable contributions of the Sun's brightness would fall close enough to the AWVR beam during portions of the tipping curve sequence. After filtering out erroneous data points, the resulting available number of data points and their temporal spacing were deemed sufficient for the purpose of the weather forecasting study [13]. This was also consistent with the number and spacing of the data points used in the previous study of 2001–2015 AWVR data [12]. The brightness temperatures were then adjusted to zenith values using the appropriate radiative transfer formulation.

During periods when an AWVR is not participating in spacecraft tracking, it continuously performs tip curves stepping at specific elevation angles between 30° and zenith (90°) at selected azimuth angles pointed away from nearby ground antennas. These data are then calibrated and examined, with various validation procedures employed prior to delivery of the data. Calibrations based on the tip curve data are conducted periodically (corresponding to activities of the Juno mission) to account for changing conditions at the AWVR site. Among several indicators, a comparison of the zenith equivalent brightness temperature is made to the cloud-free theoretical brightness temperature, which yields minimal discrepancies, thus providing validation.

Data files of time-tagged brightness temperatures (in K) at the AWVR frequency bands of 22.2, 23.8, and 31.4 GHz, as well as integrated water vapor (IWV; in cm), integrated liquid (or cloud burden; in μm), and path delay (in cm), were prepared for the Goldstone site. Retrieval algorithms for integrated water vapor were generated based on radiosonde data from the Desert Rock, Nevada site (which served as a proxy site for Goldstone). The integrated water vapor algorithm, along with the path delay and liquid water content algorithms, used the three-channel AWVR brightness temperature data as input observables. Retrieval coefficients were generated based on subsets of the radiosonde data corresponding to three parts or "seasons" of the year (November–February, March–July, and August–October) for each site, resulting in six different sets of retrieval coefficients. The output data files for Goldstone extend from January 2001 through June 2015, with significant gaps that include August–October 2006, May 2009, April 2010, August 2012, and January–July 2013 [12]. The data from 2015 to 2021 were processed separately in recent calibration sessions conducted between 2020 and 2021 for this study. A temperature control problem rendered all of the 2019 data and the first part of the 2020 data (up to the beginning of August) suspect, and thus that data was deemed unusable. There was very little or no AWVR-2 data for 2018 through much of 2020.

III. Annual Brightness Temperature Analysis

In this study, we examine and cross-compare the statistics and time-variability of the AWVR brightness temperatures and the related meteorological data types acquired between 2001 and 2021.

Table 1 lists the annual statistics for the Goldstone AWVR-2 zenith brightness temperature measurements from the 31.4 GHz channel. The first fifteen entries cover the data processed from 2001 to the first half of 2015 (January 1 to June 30), as reported in the previous study [12]. The next six entries cover the recently processed data spanning the entire period of 2015 to 2020, with the entire year of 2015 reprocessed in the same manner as the 2016 to 2020 data.

Table 1. Goldstone AWVR 31.4 GHz Brightness Temperature Statistics

Year	Average (K)	Std Dev (K)	Max (K)	Min (K)	# Points
2001	13.57	6.10	218.43	8.75	95375
2002	12.90	5.29	261.69	8.61	87346
2003	13.85	7.14	282.54	7.02	88961
2004	14.19	12.63	283.76	8.77	94411
2005	14.48	7.44	278.54	9.19	86039
2006	12.97	11.37	263.88	8.15	73392
2007	13.10	9.99	279.63	8.21	86292
2008	13.66	12.10	271.10	9.01	85995
2009	12.96	4.92	269.00	8.91	76588
2010	14.86	11.95	273.82	8.61	74445
2011	13.39	10.38	267.66	7.92	87609
2012	12.55	5.30	191.18	7.85	63325
2013	14.37	7.47	195.41	7.84	43481
2014	13.31	6.74	277.40	8.03	100178
2015	13.37	7.32	183.15	8.20	49013
2015	14.69	8.16	260.42	9.15	88116
2016	13.65	6.13	258.88	7.36	87415
2017	14.44	7.68	189.93	9.24	56613
2018	14.14	6.47	242.47	8.83	71634
2019					
2020	13.23	3.10	156.04	8.57	27518

Figure 2a displays annual cumulative distributions (CDs) of AWVR brightness temperature data from the previous study [12]. Figure 2b shows annual cumulative distributions of recent AWVR data used for the weather forecasting study [13]. The dashed black curves in Figure 2 represent the CD used by flight projects from the DSN Telecommunications Link Design Handbook [1]. There is reasonable agreement in the year-to-year CD curves and that of the DSN 810-005 curve. It is evident that the year-to-year statistics of the 31.4 GHz brightness temperatures for the 2016–2020 period are also consistent with those from the earlier study of the 2001–2015 data.

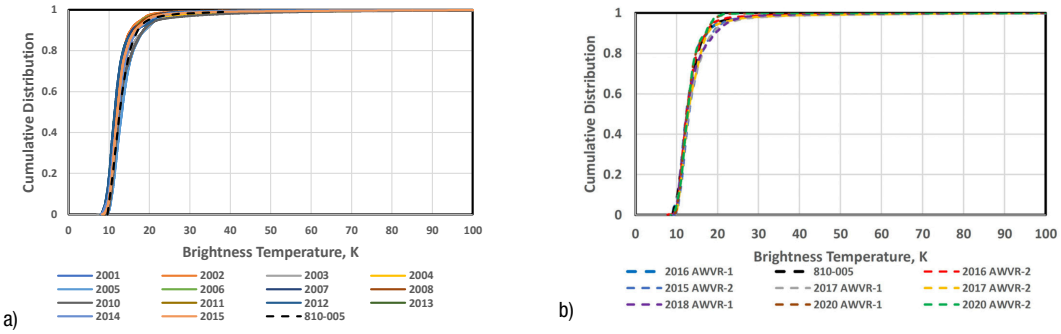

Figure 2. AWVR 31.4 GHz brightness temperature annual cumulative distributions (solid colors) along with DSN 810-005 (dashed black): a) from 2001–2015 processing report in [12], and b) from recent years processing, 2015 to 2020 (this paper).

Figure 3a shows annual CDs of the 23.8 GHz AWVR brightness temperature data from the previous study [12]. Figure 3b displays the 23.8 GHz annual CDs of the recent calibrated/processed AWVR data used in the weather forecasting study [13]. Note that both plots include 2015 data from previous calibration/processing (Figure 3a) and recent calibration/processing (Figure 3b). There is reasonable agreement in the year-to-year CD curves between the two calibration/processing sessions. Similar results were obtained for the 22.2 GHz brightness temperature channel.

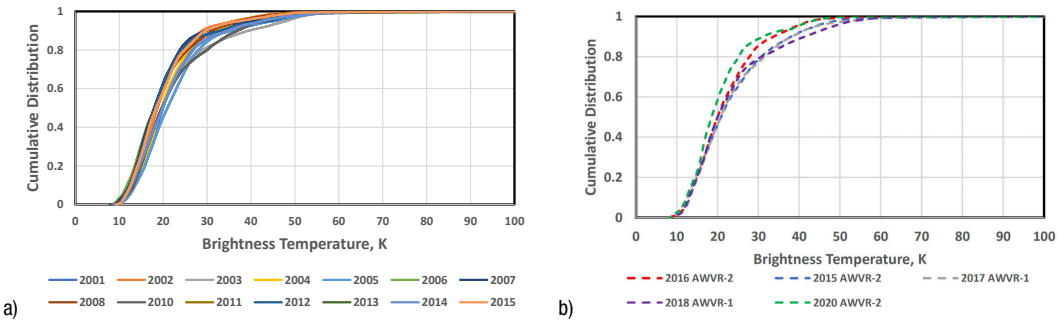

Figure 3. AWVR 23.8 GHz brightness temperature annual cumulative distributions: a) from 2001–2015 processing report in [12], and b) from recent years processing, 2015–2020 (this paper).

Figure 4 displays the annual averages of the AWVR 31.4 GHz brightness temperature data, which are tabulated in Table 1. The average of the averages is 13.57 ± 0.7 K for 2001–2015 and 14.03 ± 0.5 K for 2015–2020. There is a difference on order of 0.56 K between the means of the two calibration sessions (solid blue line for 2001–2015 and solid orange line for 2015–2020), which is within the expected calibration error of 1 K. The overall average over the full 20-year period is 13.69 ± 0.67 K, with a minimum of 12.6 K and maximum of 14.9 K. Thus, we expect a variation of about 1.5 K from the mean, some of which is likely due to true changes in the annual atmospheric conditions while some is likely due to a calibration error between annual data sets.

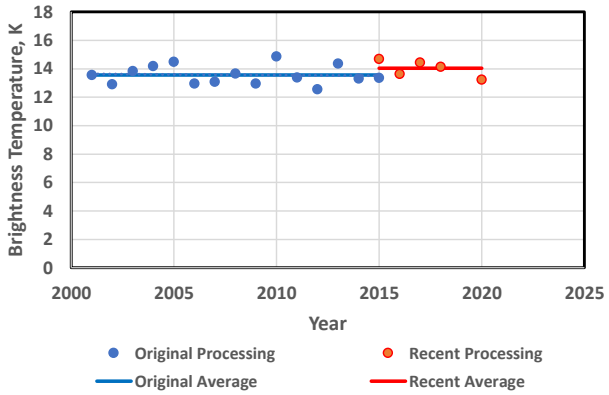

Figure 4. Average 31.4 GHz brightness temperatures derived from each year of AWVR data (see text).

Examination of the minimum 31.4 GHz brightness temperature (TB) values measured for each year at Goldstone serves to check consistency with the expected absolute minimum. The minimum value should be close to the value expected when there is an insignificant water vapor contribution, due to oxygen absorption and cosmic background only. As shown in Figure 5, almost all values fall within ±2 K of the expected absolute minimum 8.4 K due to oxygen absorption and cosmic background only (expected in absence of water vapor).

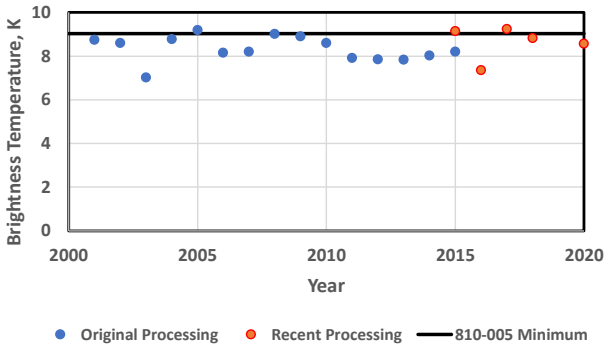

Figure 5. Minimum TB at 31.4 GHz for each year at Goldstone (2001–2015 blue points, 2015–2020 orange points) along with minimum from DSN 810-005 (black line).

IV. Annual Integrated Water Vapor

Figure 6 displays the annual cumulative distributions of IWV, where the curves for the previous study (2001–2015) are shown in solid colors and those of the recent analysis (2015–2020) are shown in dashed colors. As shown, the CDs for the recent data align well with those of the earlier study. The CD curve based on ITU global maps of IWV lies well to the right of all of the curves for CDs <70% as discussed in [12]. For the most part, the IWV averages about 1.02 cm for Goldstone. The 2001–2015 data were taken from AWVR-2 and the 2016–2020 data were taken from AWVR-1. Table 2 displays relevant statistics of the IWV measurements.

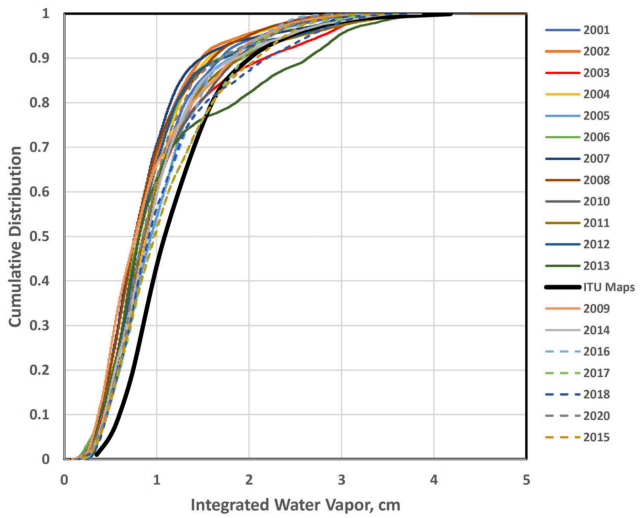

Figure 6. Annual cumulative distributions of integrated water vapor for Goldstone.

Table 2. Goldstone precipitable water vapor statistics.

Year	Number of Data Points	Average (cm)	Minimum (cm)	Maximum (cm)	90% CD (cm)	99% CD (cm)	99.9 CD (cm)
2001	94903	1.01	0.13	3.60	1.70	2.87	3.34
2002	87106	0.92	0.12	3.53	1.48	2.60	3.16
2003	88478	1.08	0.07	3.75	2.17	3.25	3.55
2004	93322	0.97	0.11	3.69	1.56	2.70	3.18
2005	85554	1.07	0.12	4.00	1.81	3.19	3.81
2006	72960	0.93	0.11	3.35	1.68	2.69	3.13
2007	85890	0.89	0.12	3.61	1.49	2.99	3.41
2008	85434	0.89	0.07	5.78	1.60	2.61	3.04
2009	76341	0.94	0.09	3.47	1.83	2.73	3.15
2010	73344	1.02	0.08	4.38	1.87	2.77	3.25
2011	87203	1.03	0.08	3.98	1.92	3.44	3.76
2012	63122	0.98	0.20	3.68	1.72	3.14	3.46
2013	43110	1.14	0.11	3.97	2.63	3.59	3.91
2014	99746	1.03	0.12	3.86	1.86	3.19	3.51
2015	80636	1.12	0.11	3.45	2.32	2.91	3.23
2016	82254	1.05	0.14	3.21	1.78	2.51	2.94
2017	49360	1.11	0.16	3.59	1.94	3.04	3.45
2018	69270	1.12	0.15	3.70	2.19	3.17	3.47
2020	44021	0.98	0.12	3.03	1.71	2.62	2.91
Overall	1462054	1.02	0.07	5.78	1.86	2.95	3.35
St. Dev.		0.08					

The ERA5 data set consists of a large number of hourly estimates of atmospheric, land, and oceanic climate variables, and covers the Earth on a 30 km grid, resolving the atmosphere over 137 levels from the surface up to 80 km [18]. Figure 7 shows the average IWV for each year from both AWVR (blue) and ERA5 (orange) analyses. The AWVR data sets from 2001

to the first half of 2015, and from 2015 (full year) to 2020 were calibrated and validated at different times using different approaches. In Table 2, we only show the IWV for the full-year reprocessing of the 2015 data. There is a 76% correlation between the ERA5 and AWVR IWV estimates (84% without 2013, a partial year), with the ERA5 curve above or near the AWVR curve except for 2013. Both data sets imply increasing water vapor trends for Goldstone (see dashed lines in Figure 7). For the ERA5 reanalysis, the monthly IWV data were at 0.25 deg horizontal resolution and interpolated at the Goldstone location.

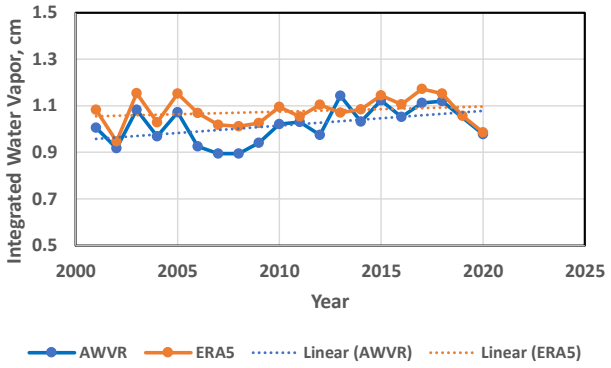

Figure 7. Integrated water vapor obtained from AWVR data (blue) and ERA5 data (orange).

We performed a preliminary assessment to determine if trends are statistically significant, where a fit to the AWVR IWV annual averages showed a slope of 0.0063 cm/year with $R^2 = 0.20$, while the ERA5 data showed a slope of 0.0023 cm/yr with $R^2 = 0.05$. The R^2 metric should not be considered significant until it attains a value of at least 0.5. To correctly assess statistical significance, all of the data from 2001 to 2020 should be calibrated using the same algorithm/techniques; this is the focus of a future study. We also plan to perform this analysis as additional years of data are acquired over a longer time span.

V. Annual Liquid Water Content

We analyzed the liquid water content extracted from the AWVR data using the available retrieval coefficients. The annual liquid water content (LWC) values from the earlier study (2001–2015) are reasonably consistent with those of the recent delivery (2015–2020) (Figure 8). The 2015 data were also recently processed, and thus both 2015 annual averages are shown, one on top of the other for the two processing sessions. In addition, different retrieval algorithms were applied in the conversion of the multifrequency brightness temperatures to LWC.

The cumulative distribution curves of LWC are shown in Figure 9. The curves from the previous study [12] are shown in solid colors while the curves for the recent data study are shown in dashed colors. For the most part, the dashed curves are generally consistent with those of the previous study. The very low LWC data point for 2020 in Figure 8 and its CD curve (dashed red) in Figure 9 are indicative of very limited data for that year.

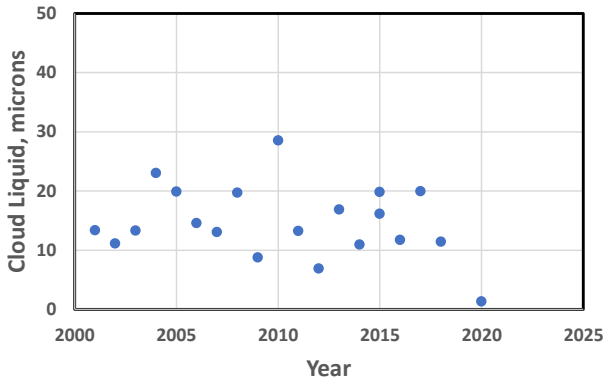

Figure 8. Average value of liquid water content for each year.

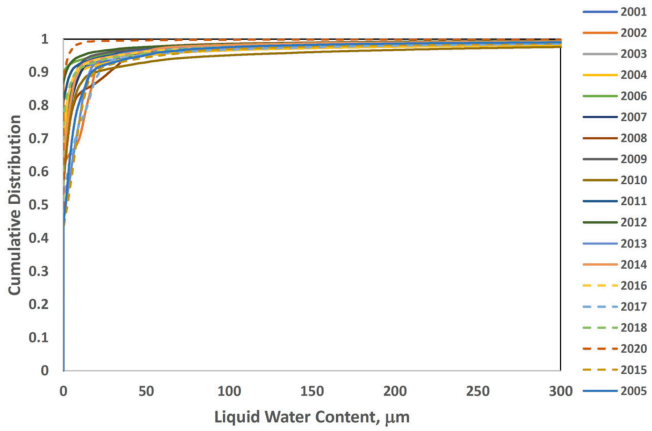

Figure 9. Annual cumulative distribution of liquid water content.

The LWC CD curves are typical for Goldstone, where about half of the time (<50%), there is little or no liquid water as evidenced by the intercept of the curves at the y-axis (LWC = 0 µm). These intercepts occur at much lower LWC values for the overseas DSN sites of Canberra and Madrid [12].

VI. Seasonal Analysis

We next examine the seasonal differences by considering a sample summer month of July throughout the ~20-year period and a sample winter month of January throughout the ~20-year period.

A. Sample Summer Month July (2001–2021)

The month of July was chosen as a sample summer month in which to compare the statistics on a yearly basis. Figure 10 displays the CD curves of the 31.4 GHz brightness temperature for July of each year. There is a span of ~3 K at the low end at 0% CD, likely due to differences in the minimum TB as July is a hot month with measurable water vapor even during the coolest periods of this month. The CD curve for year 2020 at the low end (dashed blue) likely results from a partial month containing only six days of data with

very low water vapor activity. The majority of this month's data were not used due to a temperature control problem that was diagnosed for a substantial part of the year. The CD curve for 2021 at the high end (farthest right) is a very active month involving high water vapor content. The curves for 2021 from both AWVR-1 and AWVR-2 overlap, as both data sets contain almost a full year's worth of data.

Figure 11 displays the averages and standard deviations of the 31.4 GHz brightness temperatures for the month of July for each year. The overall statistic for July is 16.83 ± 2.10 K, which, as expected, is higher than the overall annual mean of 13.7 K for all months (see Section III).

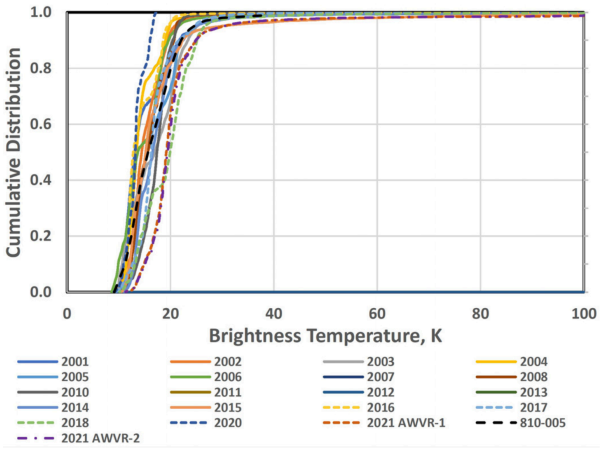

Figure 10. CD curves of 31.4 GHz brightness temperature for July of each year.

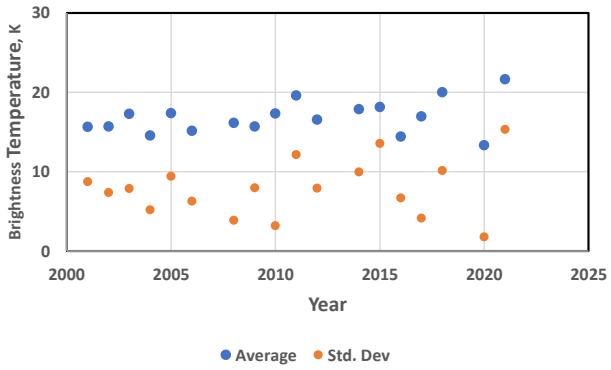

Figure 11. Averages (blue) and standard deviations (orange) for July of each year.

Figure 12 displays the minimum 31.4 GHz brightness temperatures (blue points) and the expected minimum value of 9.09 K (red line) expected due to oxygen absorption and cosmic background only. As shown, the minimum TBs are mostly within 1 K of the DSN 810-005 minimum (red line). The average of the minimum values is 9.73 ± 0.77 K. July being a hot summer month in the Goldstone climate should have more minimum TB data points above the DSN 810-005 minimum red line (due to oxygen absorption and cosmic background only). The points below the red line model are likely due to a calibration error and to a lesser extent, atmospheric variability.

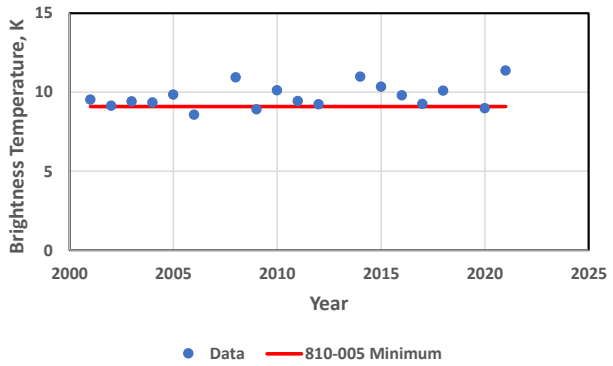

Figure 12. Minimum 31.4 GHz brightness temperature for July of each year.

The IWV averages for July of each year are shown in Figure 13. Here, the overall average is 1.82 ± 0.36 cm, above the 1.0 cm overall average (see Section IV), as expected since the desert summer climate is very hot and humid compared to the rest of the year.

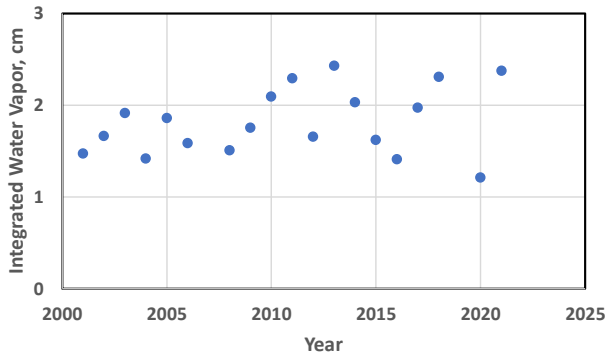

Figure 13. Average of IWV for July of each year.

B. Sample Winter Month January (2001–2021)

January was chosen as a sample winter month in which to compare the AWVR statistics on a yearly basis. Figure 14 displays the CD curves of the 31.4 GHz brightness temperatures for January of each year. The CD curves show a spread reasonably centered about the nominal DSN 810-005 curve (dashed black), suggesting consistency within ~2 K at the very low CD values (~0%) and a spread of ~16 K at the 90% CD level. Examination of the common AWVR-1 and AWVR-2 data and year-to-year statistics show consistency on order of the expected calibration error of ~1 K. Figure 15 displays the average and standard deviation of the 31.4 GHz measurements for January of each year.

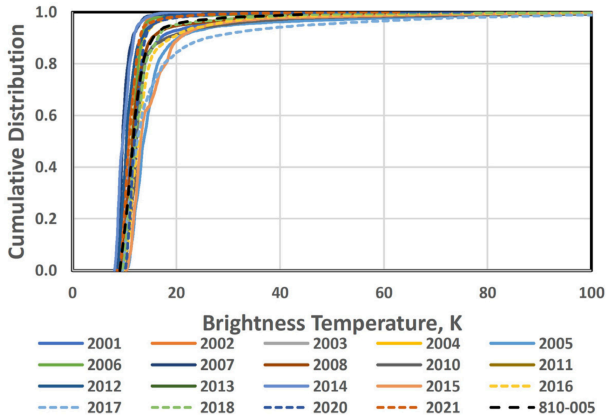

Figure 14. CD curves of 31.4 GHz brightness temperature for January of each year.

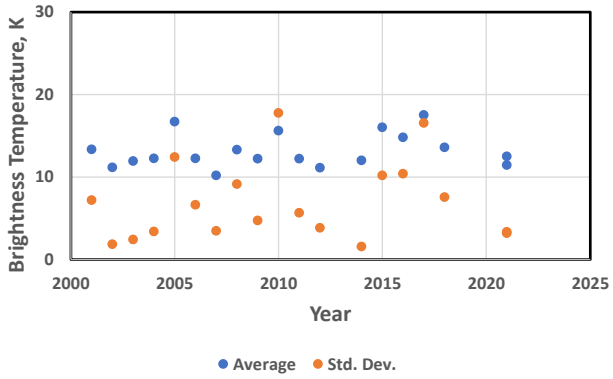

Figure 15. 31.4 GHz TB averages and standard deviations for January of each year.

Examination of minimum TB values for the winter month of January of each year (see Figure 16) allows for a consistency check with the absolute minimum expected (9.09 K) due to no water vapor (oxygen absorption only). The average minimum for January at 31.4 GHz = 9.22 ± 0.59 K. The differences of the January minimum TB values from the expected minimum (red line) are attributed to a combination of atmospheric variation and calibration error. The two points in Figure 16 for 2021 are from AWVR-1 and AWVR-2 and show a difference of ~1 K, which is consistent with the expected calibration error.

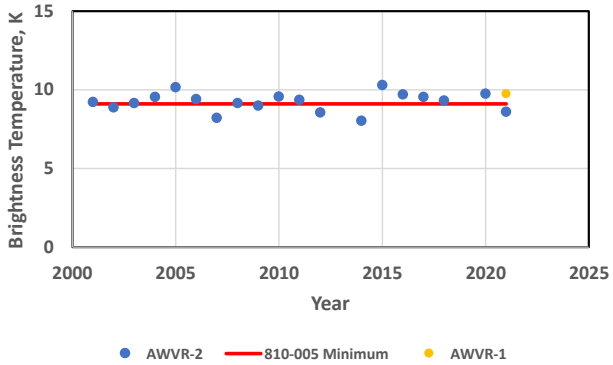

Figure 16. Minimum 31.4 GHz brightness temperature for January of each year.

Figure 17 provides an expanded scale view of the 31.4 GHz brightness temperature CDs of Figure 14. The extremities of the CD curves show very "quiet" behavior, such as during 2007 (dark blue curve at left of plot), and some instances of elevated water vapor or very active years (see 2015 (orange) and 2017 (light dashed blue) at right side of Figure 17). The time series of the 31.4 GHz for the "quiet" January of 2007 is shown in Figure 18a, while the time series for the "active" January of 2017 is shown in Figure 18b. The 31.4 GHz brightness temperatures for years 2005, 2010, and 2017 with high scatters were fairly wet years. The average brightness temperature for January at 31.4 GHz was 13.23 ± 2.16 K. Figure 19 displays the averages (blue) and standard deviations (orange) of the IWV for January of each year.

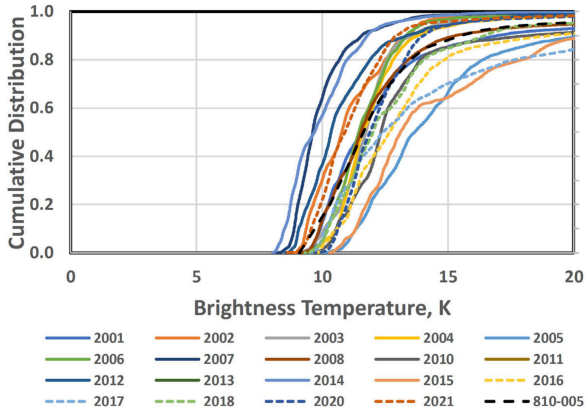

Figure 17. CD curves of 31.4 GHz brightness temperature for January of each year.

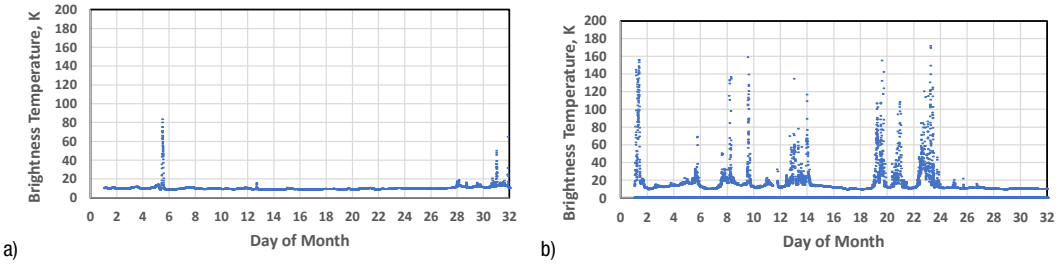

Figure 18. January time series for 31.4 GHz brightness temperature: a) for 2007, a fairly dry January, and b) for 2017, a fairly wet January.

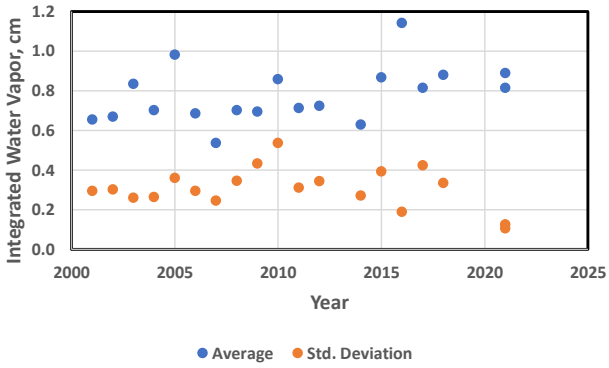

Figure 19. January statistics of IWV for each year.

VII. Conclusion

We analyzed statistics of ~20 years of AWVR brightness temperature data from 2001 to 2021, examining year-to-year consistency and discerning any trends due to calibration issues or natural variability. Recently processed data from 2015 to 2020 were used for a weather forecasting study [13]. Examination of annual cumulative distributions and statistics included a seasonal analysis using a sample summer month (July) and sample winter month (January). Table 3 lists the annual statistics for the 31.4 GHz brightness temperatures and IWV as well as for the sample winter and summer months.

Table 3. Annual and seasonal statistical summary.

	TB (31.4 GHz) (K)	IWV (cm)
Sample Winter	13.23 ± 2.10	0.78 ± 0.14
Annual	13.69 ± 0.68	1.02 ± 0.08
Sample Summer	16.83 ± 2.10	1.82 ± 0.36

We examined statistics of integrated water vapor extracted from multi-frequency AWVR brightness temperatures, where the annual IWV average of 1.02 cm was consistent with the 1.003 cm average from an earlier one-year study for Goldstone (October 5, 1993 to September 30, 1994) [19] and that inferred from a Southern California desert climate in 1977–1979 [20]. A comparison of the AWVR IWV annual means against those from ERA5 determined high correlation between both data sets. Though we performed a preliminary assessment of annual trends in average IWV, to assess statistical significance, all of the data from 2001 to 2020 should be calibrated using the same algorithm/techniques; this is the focus of a future study.

Future innovations involve using an embedded WVR (EWVR), where the WVR is integrated with the 34 m diameter BWG antenna's receiving electronics [21]. Preliminary results indicate that atmospheric water vapor can be measured using a standard DSN receiver without compromising telecommunication performance and allowing for the correction of tropospheric path delay variability in spacecraft tracking data, as well as continuously monitoring the atmospheric noise temperature contributions [21].

This article is the companion full paper of a poster that was presented at the 2021 Fall Meeting of the American Geophysical Union [22].

Acknowledgments

We would like to thank Alan Tanner of the Jet Propulsion Laboratory for consultation on AWVR calibration issues. We also thank Laurence Snedeker of DSN Operations for providing the photograph of the AWVRs for Figure 1. We also acknowledge funding provided by the Research and Technology Development (R&TD) program at the Jet Propulsion Laboratory in Pasadena, California. The research was carried out at the Jet Propulsion Laboratory, California Institute of Technology, under a contract with the National Aeronautics and Space Administration (80NM0018D0004).

References

[1] S. D. Slobin, "Atmospheric and Environmental Effects," *DSN Telecommunications Link Design Handbook,* DSN No. 810-005, Space Link Interfaces, Module 105, Rev. E, Jet Propulsion Laboratory, Pasadena, California, issue date October 22, 2015. http://deepspace.jpl.nasa.gov/dsndocs/810-005/105/105E.pdf

[2] B. Bertotti, L. Iess, and P. Tortora, "A Test of General Relativity Using Radio Links with the Cassini Spacecraft," *Nature,* vol. 425, no. 6956, pp. 374–376, September 25, 2003.

[3] D. Buccino, M. Parisi, D. S. Kahan, M. Paik, Y. M. Yang, W. M. Folkner, and K. Oudrhiri, "Impact of the Advanced Water Vapor Radiometer on the Juno Gravity Science Investigation," in *AGU Fall Meeting Abstracts*, vol. 2019, pp. P34A-07, December 2019.

[4] R. P. Linfield, L. P. Teitelbaum, L. J. Skjerve, S. J. Keihm, S. J. Walter, M. J. Mahoney, and R. N. Treuhaft, "A Test of Water Vapor Radiometer–Based Troposphere Calibration Using VLBI Observations on a 21-Kilometer Baseline," *The Telecommunications and Data Acquisition Progress Report,* vol. 42-122, Jet Propulsion Laboratory, Pasadena, California, pp. 12–31, April–June 1995, article dated August 15, 1995. http://ipnpr.jpl.nasa.gov/progress_report/42-122/122I.pdf

[5] S. J. Keihm, M. A. Janssen, and C. S. Ruf, "TOPEX/Poseidon Microwave Radiometer (TMR): III. Wet Troposphere Range Correction Algorithm and Pre-Launch Error Budget," *IEEE Transactions on Geoscience and Remote Sensing,* vol. 33, no. 1, January 1995.

[6] A. Tanner, "Development of a high-stability water vapor radiometer," *Radio Science,* vol. 33, no. 2, pp. 449–462, March–April 1998. https://agupubs.onlinelibrary.wiley.com/doi/pdf/10.1029/97RS02749

[7] W. L. Flock, S. D. Slobin, and E. K. Smith, "Propagation Effects of Radio Range and Noise in Earth–Space Telecommunications," *Radio Science,* vol. 17, no. 6, pp. 1411–1424, November–December 1982.

[8] G. Elgered, "Tropospheric Radio Path Delay From Ground-Based Microwave Radiometry," Chapter 5, *Atmospheric Remote Sensing by Microwave Radiometry*, edited by M. Janssen, New York: Wiley & Sons, 1993.

[9] D. D. Morabito, L. R. D'Addario, R. J. Acosta, and J. A. Nessel, "Tropospheric Delay Statistics Measured by Two Site Test Interferometers at Goldstone, California," *Radio Science,* vol. 48, 2013, doi:10.1002/2013RS005268. http://onlinelibrary.wiley.com/doi/10.1002/2013RS005268/abstract

[10] D. D. Morabito, L. R. D'Addario, S. Keihm, and S. Shambayati, "Comparison of Dual Water Vapor Radiometer Differenced Path Delay Fluctuations and Site Test Interferometer Phase Delay Fluctuations Over a Shared 250-Meter Baseline," *The Interplanetary Network Progress Report,* vol. 42-188, Jet Propulsion Laboratory, Pasadena, California, pp. 1–21, February 15, 2012. http://ipnpr.jpl.nasa.gov/progress_report/42-188/188A.pdf

[11] D. D. Morabito, "A Comparison of Estimates of Atmospheric Effects on Signal Propagation Using ITU Models: Initial Study Results," *The Interplanetary Network Progress Report,* vol. 42-199, Jet Propulsion Laboratory, Pasadena, California, pp. 1–24, November 15, 2014. http://ipnpr.jpl.nasa.gov/progress_report/42-199/199D.pdf

[12] D. D. Morabito, S. Keihm, and S. Slobin, "A Statistical Comparison of Meteorological Data Types Derived from Deep Space Network Water Vapor Radiometers," *The Interplanetary Network Progress Report,* vol. 42-203, Jet Propulsion Laboratory, Pasadena, California, November 15, 2015. https://ipnpr.jpl.nasa.gov/progress_report/42-203/203A.pdf

[13] L. Wu, D. D. Morabito, L. Huang, J. P. Teixeira, H. M. Nguyen, H. Su, M. A. Soriano, L. Pan, and D. S. Kahan, "Prediction of Atmospheric Noise Temperature at the Deep Space Network with Machine Learning," *AGU Fall Meeting 2021,* New Orleans, LA, 2021.

[14] D. D. Morabito, L. Wu, and S. Slobin, "A Comparison of Atmospheric Quantities Determined from Advanced WVR and Weather Analysis Data," *The Interplanetary Network Progress Report,* vol. 42-209, Jet Propulsion Laboratory, Pasadena, California, May 15, 2017. https://ipnpr.jpl.nasa.gov/progress_report/42-209/209B.pdf

[15] G. M. Resch, J. E. Clark, S. J. Keihm, G. E. Lanyi, C. J. Naudet, A. L. Riley, H. W. Rosenberger, and A. B. Tanner, "The Media Calibration System for Cassini Radio Science: Part II," *The Telecommunications and Mission Operations Progress Report,* vol. 42-145, pp. 1–20, May 15, 2001. https://ipnpr.jpl.nasa.gov/progress_report/42-145/145J.pdf

[16] J. Oswald, L. Riley, A. Hubbard, H. Rosenberger, A. Tanner, S. Keihm, C. Jacobs, G. Lanyi, and C. Naudet, "Relocation of Advanced Water Vapor Radiometer 1 to Deep Space Station 55," *The Interplanetary Network Progress Report,* vol. 42-163, Jet Propulsion Laboratory, Pasadena, California, pp. 1–6, November 15, 2005. https://ipnpr.jpl.nasa.gov/progress_report/42-163/163C.pdf

[17] S. Asmar, S. Bolton, D. Buccino, T. Cornish, W. Folkner, R. Formaro, L. Iess, A. Jongeling, D. Lewis, A. Mittskus, R. Mukai, and L. Simone, "The Juno Gravity Science Instrument," *Space Science Reviews*, vol. 213. 1-14. 10.1007/s11214-017-0428-7.

[18] H. Hersbach, B. Bell, P. Berrisford, S. Hirahara, A. Horányi, J. Muñoz-Sabater, J. Nicolas, C. Peubey, R. Radu, D. Schepers, A. Simmons, C. Soci, S. Abdalla, X. Abellan, G. Balsamo, P. Bechtold, G. Biavati, J. Bidlot, M. Bonavita, G. Chiara, P. Dahlgren, D. Dee, M. Diamantakis, R. Dragani, J. Flemming, R. Forbes, M Fuentes, A. Geer, L. Haimberger, S. Healy, R. J. Hogan, E. Hólm, M. Janisková, S. Keeley, P. Laloyaux, P. Lopez, C. Lupu, G. Radnoti, P. Rosnay, I. Rozum, F. Vamborg, S. Villaume, and J. N. Thépaut, "The ERA5 global reanalysis," *Quarterly Journal of the Royal Meteorological Society*, vol. 146, pp. 1999–2049. https://doi.org/10.1002/qj.3803

[19] S. J. Keihm, "Water Vapor Radiometer Measurements of the Tropospheric Delay Fluctuations at Goldstone Over a Full Year," *The Telecommunications and Data Acquisition Progress Report,* vol. 42-122, April–June 1995, Jet Propulsion Laboratory,

Pasadena, California, pp. 1–11, August 15, 1995.
http://ipnpr.jpl.nasa.gov/progress_report/42-122/122J.pdf

[20] A. L. Berman and S. D. Slobin, "Tropospheric Path Length Fluctuation in Temperate Semiarid Locales: Application to the Gravitational Wave Experiment," *The Deep Space Network Progress Report,* vol. 42-55, Jet Propulsion Laboratory, Pasadena, California, November–December 1979, February 15, 1980.
http://ipnpr.jpl.nasa.gov/progress_report2/42-55/55L.PDF

[21] A. B. Tanner, J. S. Border, A. P. Jongeling, E. M. Long, E. Pereira, and E. Lin, "Embedding a Water Vapor Radiometer Within a Deep Space Network Ka-band Receiver," *The Interplanetary Network Progress Report,* vol. 42-226, Jet Propulsion Laboratory, Pasadena, California, pp. 1–17, August 15, 2021.
https://ipnpr.jpl.nasa.gov/progress_report/42-226/42-226F.pdf

[22] D. D. Morabito, D. Kahan, M. Paik, L. Wu, E. Barbinis, D. Buccino, and M. Parisi, "A Study of Twenty Years of Advanced Water Vapor Radiometer Data at Goldstone, California," *AGU Fall Meeting 2021,* New Orleans, LA, 2021.